Revealing the Magnetic Order in a New Dirac Antiferromagnet $EuMnBi_2$ by Resonant X-Ray Magnetic Scattering

Dirac materials, in which the low-energy excitation is described as relativistic Dirac fermions, have attracted considerable attention because of the fascinating magnetotransport associated with the extremely high mobility. We report on a new layered Dirac antiferromagnet $EuMnBi_2$, where we observed the bulk half-integer quantum Hall effect as a consequence of the exquisite combination of Dirac fermions and Eu magnetic moments in a natural superlattice structure. By systematic measurements of resonant X-ray scattering at BL-3A, we have succeeded in revealing the detailed magnetic structure of the Eu sublattice, which is of great importance to understand the mechanism of novel quantum transport of Dirac fermions strongly coupled with magnetism.

Dirac fermions in solids have recently attracted significant attention as a new electronic state that is described by the relativistically massless Dirac equation. In 2005, the experimental discovery of the half-integer quantum Hall effect (QHE) in graphene triggered worldwide researches on novel quantum magnetotransport of Dirac fermions. For potential application to spintronic devices, it is essential to know how the transport of Dirac fermions is controlled by magnetic order in a solid as well as by external fields, which has remained elusive so far. Although a variety of Dirac materials have been recently discovered, the quantum transport phenomena relevant to Dirac fermions were observable mostly in nonmagnetic compounds.

To explore magnetic Dirac materials, in this study we focused on a layered bulk antiferromagnet $EuMnBi_2$. Recently, layered magnets AMnBi$_2$ (A = Sr^{2+} [1-3] and Eu^{2+} [4, 5]) were found to host anisotropic 2D Dirac fermions, providing an ideal arena in which to examine the interplay between Dirac fermions and ordered magnetic moments. The crystal structure consists of the conducting layers of Bi square net hosting quasi two-dimensional (2D) Dirac fermions and the insulating magnetic layers consisting of the Mn-Bi and A layers (**Fig. 1A**). From detailed magnetic and transport measurements on $EuMnBi_2$, intriguingly we have discovered that the quantum transport properties of Dirac fermions are strongly coupled with the antiferromagnetic order of the Eu sublattice, as detailed below [6]. We report on the detailed magnetic structure of the Eu sublattice, which is indispensable to understand the mechanism of the correlated magnetotransport of Dirac fermions. For this purpose, we have performed resonant X-ray scattering measurements at BL-3A, by utilizing horizontally polarized X-rays in resonance with the Eu L_3 absorption edge (~6.975 keV).

First, we briefly present the magnetic and transport features for $EuMnBi_2$. As shown in **Fig. 2A**, the magnetic susceptibility M/H parallel to the c axis for $EuMnBi_2$ steeply decreases below the antiferromagnetic (AFM) transition temperature T_N ~ 22 K, indicating that the Eu moments are aligned parallel to the c axis. At T_N, we observed a steep jump in interlayer resistivity ρ_{zz} toward the lowest temperature (**Fig. 2C**). The orientation of the ordered Eu moments can be controlled by applying magnetic fields; the magnetization at 1.9 K exhibits a clear metamagnetic (spin-flop) transition at $H = H_f$ (~5.3 T), corresponding to the reorientation of the Eu moments to be perpendicular to the field (**Fig. 1B** and its inset). Above H_f, interestingly, ρ_{zz} increases by about one order of magnitude, followed by giant Shubnikov–de Haas (SdH) oscillations that reach $\Delta\rho_{osc}/\rho$ ~50%. In such a high-ρ_{zz} state, we observed plateau-like structures in the Hall resistivity, which is the first observation of the multilayer half-integer quantum Hall effect of quasi 2D Dirac fermions in a bulk magnet (data not shown) [6].

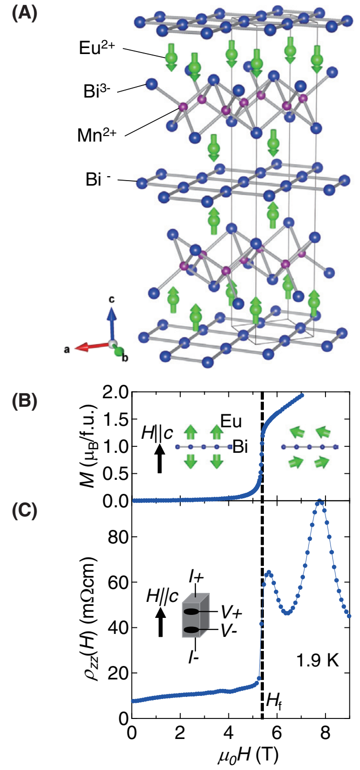

Figure 1: (A) Schematic illustration of the crystal and magnetic structures for $EuMnBi_2$ at zero field, together with the formal valence of each ion. The magnetic moments of the Mn sublattice are not shown for brevity. **(B & C)** Magnetic field dependence of magnetization M **(B)** and interlayer resistivity ρ_{zz} **(C)** at 1.9 K. The inset to **(B)** shows a schematic illustration of the Eu^{2+} moments adjacent to the Bi layer for each antiferromagnetic (AFM) phase. A schematic sample configuration for the interlayer resistivity measurement is presented in the inset to **(C)**. H_f corresponds to the transition field to the spin-flop AFM phase.

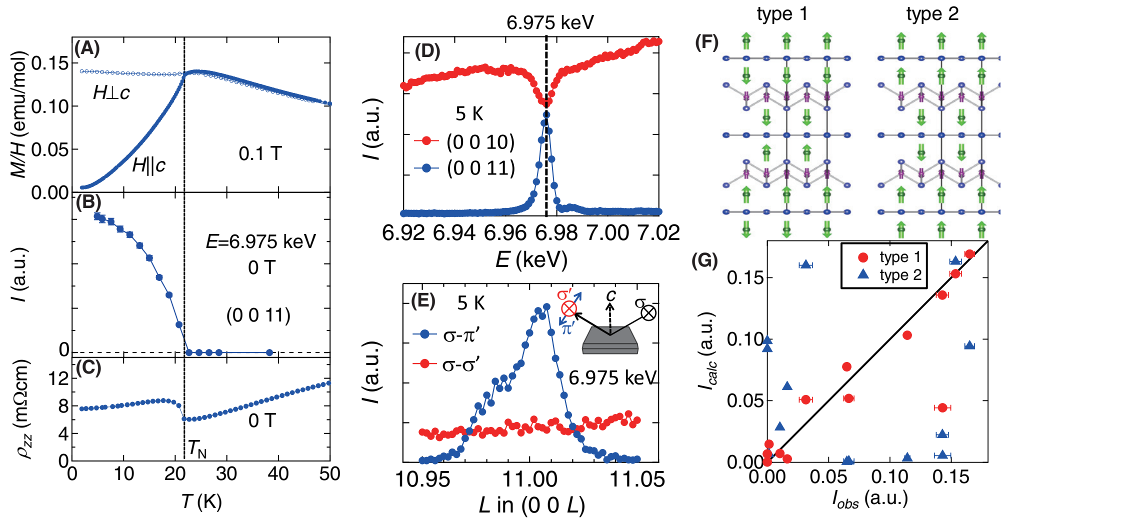

Figure 2: (A to **C)** Temperature profile of magnetic susceptibility M/H at 0.1 T **(A)**, intensity of the resonant magnetic reflection (0 0 11) at 6.975 keV at 0 T **(B)**, and interlayer resistivity ρ_{zz} at 0 T **(C)**. T_N denotes the AFM transition temperature. **(D)** Energy profiles of the (0 0 10) Bragg reflection and (0 0 11) magnetic reflection with σ-incident polarization at 5 K. The resonant energy is 6.975 keV. **(E)** Profile of the (0 0 11) magnetic reflection along [001] at 5 K at 6.975 keV for the σ-π' configuration (blue) and σ-σ' configuration (red). Inset shows a schematic illustration of the experimental setup. **(F)** Two types of antiferromagnetic order of the Eu sublattice at 5 K. **(G)** Comparison between the observed (I_{obs}) and calculated (I_{calc}) intensities of the (0 0 L=odd) and (1 0 L=even) magnetic reflections at 5 K for each type of antiferromagnetic order.

In the resonant X-ray scattering spectra near the Eu L_3 absorption edge, we found the (0 0 11) reflection at E = 6.975 keV, which is forbidden in the present space group ($I4/mmm$). Considering the evolution of the intensity below T_N (**Fig. 2B**) and the sharp resonance at the Eu L_3 edge (**Fig. 2D**), it can be assigned to resonant magnetic scattering from the Eu sublattice. Furthermore, the magnetic origin of the (0 0 11) reflection was ensured by polarization analyses as follows. The magnetic form factor (f_i^{mag}) of the ith Eu magnetic moment in the electric-dipole transition is described as

$$f_i^{\mathrm{mag}} \propto (\boldsymbol{e} \times \boldsymbol{e}') \cdot \widehat{\boldsymbol{m}}_{\boldsymbol{i}},$$

where $\boldsymbol{e}$ and $\boldsymbol{e}'$ denote unit vectors of the incident and scattered polarization, respectively, and $\widehat{\boldsymbol{m}}_{\boldsymbol{i}}$ unit vector of the ith Eu magnetic moment. Based on this equation, the (0 0 L) magnetic scattering should appear only in the rotated σ-π' channel. As shown in **Fig. 2E**, the (0 0 11) reflection was indeed observed in the σ-π' configuration but not in the σ-σ' configuration.

Finally, we discuss the antiferromagnetic order pattern of the Eu sublattice at zero field. The observation of (0 0 11) reflection indicates that the Eu magnetic moments order ferromagnetically within the ab plane and antiferromagnetically along the c axis, resulting in two kinds of AFM order as possible candidates (type 1 and 2 in **Fig. 2F**). To determine the order arrangement, we have measured the intensities (I_{obs}) of several (0 0 L) (L=odd) and (1 0 L) (L=even) magnetic reflections and compared them with the calculated intensities I_{calc} for type 1 and 2 (**Fig. 2G**). Measured intensities are in excellent agreement with the calculation results for type 1, indicating that the most probable Eu moment arrangement is type 1.

The obtained crystal and magnetic structure of $EuMnBi_2$ is regarded as a natural spin-valve structure embedded in a multilayer Dirac fermion system, as shown in **Fig. 1A**. This indicates that the interlayer conduction is suppressed by the staggered Eu moments along the c axis, whereas the ferromagnetic order within the plane may promote the in-plane transport, leading to extremely high carrier mobility of ~14,000 cm^2/V at 2 K. Our discovery opens the door for engineering the Dirac fermion transport in magnetic materials suitable for novel spintronic devices with an extremely high speed.

REFERENCES

[1] J. Park, G. Lee, F. Wolff-Fabris, Y. Y. Koh, M. J. Eom, Y. K. Kim, M. A. Farhan, Y. J. Jo, C. Kim, J. H. Shim and J. S. Kim, *Phys. Rev. Lett.* **107**, 126402 (2011).
[2] J. K. Wang, L. L. Zhao, Q. Yin, G. Kotliar, M. S. Kim, M. C. Aronson and E. Morosan, *Phys. Rev. B* **84**, 064428 (2011).
[3] K. Wang, D. Graf, H. Lei, S. W. Tozer and C. Petrovic, *Phys. Rev. B* **84**, 220401(R) (2011).
[4] A. F. May, M. A. McGuire and B. C. Sales, *Phys. Rev. B* **90**, 075109 (2014).
[5] S. Borisenko, D. Evtushinsky, Q. Gibson, A. Yaresko, T. Kim, M. N. Ali, B. Buechner, M. Hoesch and R. J. Cava, *arXiv*: 1507.04847 (2015).
[6] H. Masuda, H. Sakai, M. Tokunaga, Y. Yamasaki, A. Miyake, J. Shiogai, S. Nakamura, S. Awaji, A. Tsukazaki, H. Nakao, Y. Murakami, T.-H. Arima, Y. Tokura and S. Ishiwata, *Sci. Adv.* **2**, e1501117 (2016).

BEAMLINE

BL-3A

H. Sakai[1, 2], H. Masuda[2], Y. Yamasaki[2, 3], H. Nakao[4], Y. Murakami[4], T.-H. Arima[2, 3], Y. Tokura[2, 3] and S. Ishiwata[2, 5] ([1]Osaka Univ., [2]The Univ. of Tokyo, [3]RIKEN-CEMS, [4]KEK-IMSS-PF/CMRC, [5]PRESTO)